Archives of Materials Science and Engineering

Volume 112
Issue 1
November 2021
Pages 23-31

International Scientific Journal published monthly by the World Academy of Materials and Manufacturing Engineering

DOI: 10.5604/01.3001.0015.5929

Influence of welding parameters on decarburization in heat affected zone of dissimilar weldments after post weld heat treatment

M.O. Nimko
E.O. Paton Electric Welding Institute NASU, 11 Malevich St., Kiev 03680, Ukraine
* Corresponding e-mail address: maxim.nimko@gmail.com
ORCID identifier: https://orcid.org/0000-0002-9672-4921

ABSTRACT

Purpose: This paper aims to assess an influence of thermal welding parameters on microstructural evolution in the weld adjacent zone of P91 steel, overlayed by austenitic consumables, after post weld heat treatment.

Design/methodology/approach: Analysis of the width of decarburized layer on microphotographs of overlayed specimens after tempering 750°C, 7 and 18 hours. Specimens were made by using different heat input and preheating temperature parameters.

Findings: It is shown that with increase of the heat input energy, the width of the resulting decarbonized layer decreases linearly; the effect of heating temperature on the layer width is parabolic with a minimum at a temperature of ~195°C.

Research limitations/implications: Future research may include comparison of the creep rupture strength of the weldments, made with different welding parameters, to assess the influence of kinetics of decarburization and variation of the parameters on creep rupture strength.

Practical implications: Results permit to achieve minimization of rate of carbon diffusion in the weld adjacent zone of the HAZ by means of variation of welded parameters.

Originality/value: Experimentally was confirmed a role of high-diffusivity paths (grain boundaries) on carbon diffusion in the HAZ of dissimilar weldments; found correlation between welding parameters and the rate of the diffusion during high temperature exposure.

Keywords: Welding, Dissimilar welds, Carbon diffusion, Grain boundaries

Reference to this paper should be given in the following way:

M.O. Nimko, Influence of welding parameters on decarburization in heat affected zone of dissimilar weldments after post weld heat treatment, Archives of Materials Science and Engineering 112/1 (2021) 23-31. DOI: https://doi.org/10.5604/01.3001.0015.5929

MATERIALS MANUFACTURING AND PROCESSING

© Copyright by International OCSCO World Press. All rights reserved. 2021

1. Introduction

The main thermodynamic cycle of thermal power plants used in modern power industry is the Rankine cycle with superheated steam [1]. To implement this thermal cycle, different sections of the steam-water circuit at the power plant must have different parameters of temperature and pressure of the working fluid. In order to reduce the cost of construction in modern power plants, areas with lower steam parameters are made of low-alloy bainitic steels with 0.5…2.25% Cr (water wall tubes; temperatures up to 600°C) and martensitic steels with 9…12% Cr (upper sections of tube of water wall, header, steam pipeline; temperatures to 625-630°C); areas with even higher steam parameters – from more expensive austenitic steels (superheaters; temperatures up to 660-680°C) [1]. In particular, in the superheater sections of a modern thermal power plant, operating at a temperature of 600°C, there are 4674 welded joints between martensitic steels with 9% Cr and austenitic steels [2].

Since ferritic steels have a higher carbon content than austenitic, the concentration gradient of carbon in the contact zone of these steels decreases from ferritic steel in the austenitic direction. At elevated temperatures, carbon diffuses in the direction of lowering the chemical potential gradient. It is important to note that chromium reduces the chemical potential of carbon [3,4], while the chromium content increases from ferritic-martensitic steel to austenitic. Therefore, the gradients of chromium and carbon concentrations create a rather sharp gradient of chemical potential across the fusion zone. In addition, the carbon diffusion coefficient in ferrite is much higher than in austenite, while the solubility of carbon is lower. The result of these factors is a strong driving force for the diffusion of carbon from ferritic steel to austenitic, which results in the formation of a decarburized layer in ferritic steel, what corresponds to a significant reduction in hardness [3,5].

The result of decarburization of low-alloy steel in the areas, adjacent to the weld line, is the dissolution of carbides $M_{23}C_6$ and M_7C_3 [5], which can occur on the background of carbides dissolution and transformation during high temperature exposure [6,7]. The resulting loss of microstructural stability in the decarburized layer can lead to excessive recovery of the dislocation structure and recrystallization (this is generally confirmed in the case of joints made between steels of the 2¼Cr-1Mo and 9Cr-1Mo grades [8-10]). The decarburized layer has lower mechanical properties, which, for example, can be characterized by a decrease in hardness and a high concentration of localized deformation accumulation, measured during the tensile test [5]. However, the loss of the long-term hardening mechanism due to the dissolution of carbides, which reduces the dispersion hardening, and the recrystallization of the bainite structure, which eliminates the combined effect of dislocation and subgrain boundary hardening, is an important aspect of degradation; destruction within the decarburized layer has also been reported [5, 11-14].

In turn, a more carbonized layer is formed in higher alloyed steel. In work [15] it was shown that microcracks can arise in such a carburized layer. Microcracks mainly originate in the transition zone and have an intergranular character. A similar process of crack formation in the carburized layer after heat treatment is described in [16,17].

Therefore, it is necessary to reduce the decarburized layer in the dissimilar joints during high-temperature operation in creep conditions. It is generally accepted to use nickel-based filler materials to reduce carbon migration in such joints. However, most researchers believe that traditional nickel-based materials (alloy 82/182/617/625, etc.) cannot effectively and completely inhibit the diffusion of carbon from martensitic steel into the weld, because most nickel alloys, used as welding materials, contain a large number of carbide-forming elements [18-26].

Problems concerning evolution of the microstructure in dissimilar weldments between martensitic and austenitic steels still attract attention of researchers worldwide, the most recent literature reviews include [27-30]. Recent case studies focus both on traditional combinations of materials [31], and on newly developed materials and combinations [25,32], applied in different industries.

In this work, we have studied the effect of thermal welding parameters (heat input energy and associated heating temperature) on the diffusion kinetics of carbon in the weld-adjacent zone of dissimilar joints.

2. Experimental procedure and results

Overlaying welding was made on 20 mm thick plates of martensitic Grade 91 steel by austenitic welding material, which was chosen to create a difference in chemical composition. Such joints can be found in connections between header (P91) and superheaters (austenitic steels) in operating power plants. To eliminate the effect of reheating, overlaying was made with single pass. The chemical compositions of the base metals and the filler materials are given in Table 1.

Overlaying was performed by: a) changing the heat input at room temperature; b) changing the preheating temperature at approximately the same heat input temperature.

Table 1.
Chemical compositions of base and filler materials used, mass contents in %

Element	P91 steel	Fox CN 23/12 Mo-A
C	0.1	0.01
Si	0.34	0.63
Mn	0.47	0.73
Cr	8.52	23.0
Ni	0.28	13.1
Mo	0.93	2.6
V	0.2	-
Nb	0.072	-
N	0.06	-

The last point was included due to the following reason: although P91 steel is usually welded with austenitic materials without preheating, but due to different heat input, depending on the overlaying parameters, the so-called autoheating (as a result of the concurrent heating) can occur with different values of maximum temperature.

Overlaying conditions are listed in Table 2. The heat input q was calculated by the formula

$$q = \frac{\eta \cdot I \cdot U}{V} \quad (1)$$

where η is the efficiency of the welding method (took η = 0.85); I – current strength, A; U – arc voltage, V (took U ≈ 24 V).

Table 2.
Parameters of overlaying

Current strength, A	Welding rate, m/h	Heat input, kJ/m	Preheating, °C
1) variation of current strength and welding rate			
100	18.67	393	20
120	14.40	612	
140	11.39	903	
2) variation of preheating temperature			
120	14.40	612	20
	15.63	564	150
	15.16	581	300

After overlaying, the plates were cut into three templates (Fig. 1), two of which were tempered at 750°C for 7 and 18 h to intensify the processes of carbon diffusion and the formation of a decarburized layer. From the templates in the state after welding and after tempering, metallographic sections were made. The sample in the state after welding was chemically etched with 15% HNO_3 acid solution to detect grain boundaries, the samples in the state after tempering were electrolytically etched in H_2CrO_4 for 15 s at 10 V voltage to detect the decarburized layer.

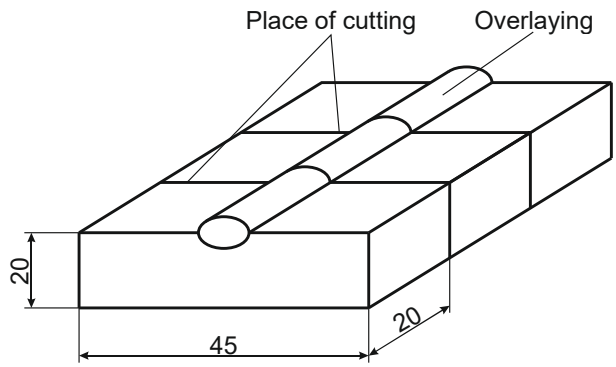

Fig. 1. Scheme of cutting of templates

In the literature, for example [33], the notion of the effective thickness of the diffusion layer is used, which is determined by the shortest distance from the saturation surface (e.g., the fusion line) to the measurement area, which is characterized by the determinate nominal value of a basic parameter. The basic parameter is either the concentration of the diffusing element, or a mechanical property (hardness), or a structural feature, such as low etch ability of this area.

To determine the average width of the decarburized layer in the tempered overlayed templates, panoramic micrographs of the structure were taken along the fusion line at x100 magnification, and 6 to 11 micrographs were obtained for each type of joints, depending on the width of the overlaying bead. Measurement of the area of poorly etched weld-adjacent area and the length of the fusion line was performed using free software ImageJ [34]. Based on the measurement results, histograms were constructed for the cases of variation of heat input energy and preheating temperature. Each column of histograms reflects the width of the decarbonized layer on a particular micrograph, the columns are arranged in the order of shooting of micrographs from the left edge of the roller to the right (Fig. 2).

The average values of the width of the diffusion layer P for each bead (dashed line on histograms) were determined by the formula

$$P = \frac{\sum_{i=1}^{n}(p_i \cdot l_i)}{\sum_{i=1}^{n} l_i} \quad (2)$$

where p_i is the width of the diffusion layer (μm) on a certain micrograph i (n is the total number of microphotographs for a bead), l_i is the length of the fusion line (μm) on a certain micrograph i.

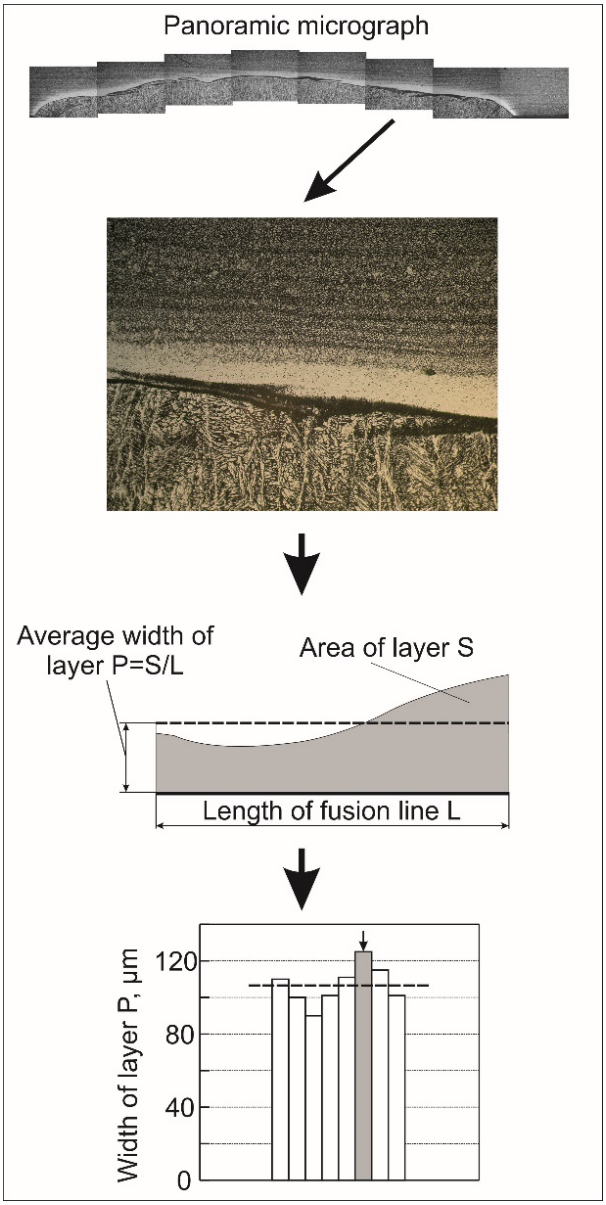

Fig. 2. Scheme of histogram constructing

The results of experiments and their analysis

Figure 3 show examples of micrographs of the weld-adjacent zone of steel P91 in the state after tempering 750°C, 7 and 18 h, respectively. In the microphotographs it is possible to note a significant range of fluctuations in the width of the decarburized layer at the same temperature exposure.

Figure 4 demonstrates histograms for width of the decarburized layer depending on overlaying parameters after tempering 750°C, 7 and 18 h, constructed according to the method, described above.

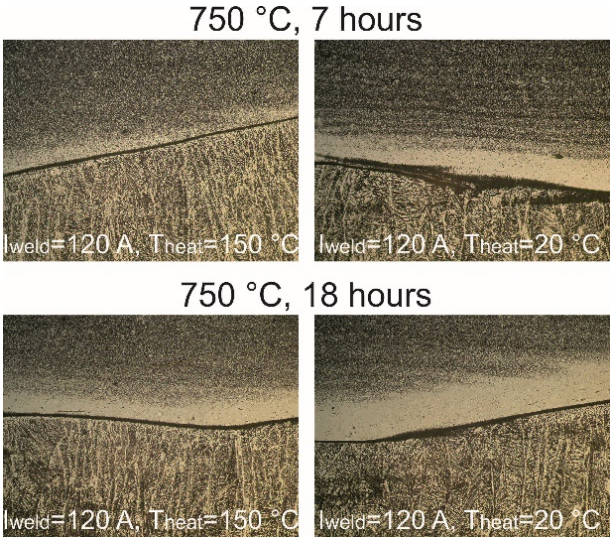

Fig. 3. Examples of microphotographs to determine the width of the layer depending on the welding mode after tempering 750°C, 7 and 18 h, x100

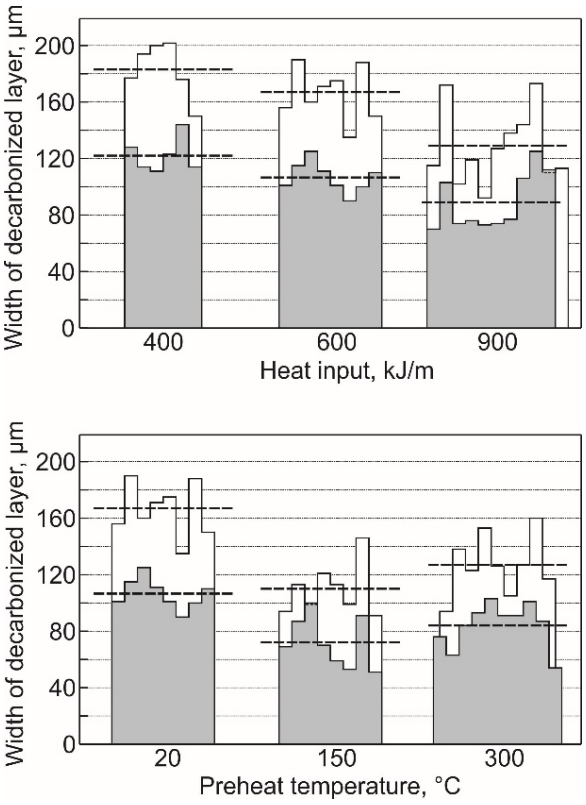

Fig. 4. Dependences of the width of the decarburized layer on the welding parameters in the weld-adjacent zone of P91 steel after tempering at 750°C, 7 h (grey area) and 18 h (white area)

Figure 5 shows a graphical analysis of the distribution of the average width values of the decarburized layers. It is shown that in the considered range of heat input energies 400… 900 kJ/m the decrease in the width of the diffusion layer after tempering for 7 and 18 h occurs almost linearly with increasing value of the heat input used in SMAW. Approximating line in Figure 5, a is determined by the least squares method.

It is noted that with increase of preheating temperature, the width of the layer after PWHT first decreases, then begins to increase again (Fig. 5b). If we approximate the experimental data using the quadratic model $A \cdot T^2+B \cdot T+C$ (where T is the preheating temperature (°C); A, B, C – coefficients that can be found using a computer algebra system), differentiate the equation model and find its root, we can determine the value of the minimum temperature at which the diffusion layer will be the smallest. In our case, after 7 hours of tempering, the minimum occurs at 193°C, after 18 hours – at 196°C. The temperature of 195°C was taken as a rough average.

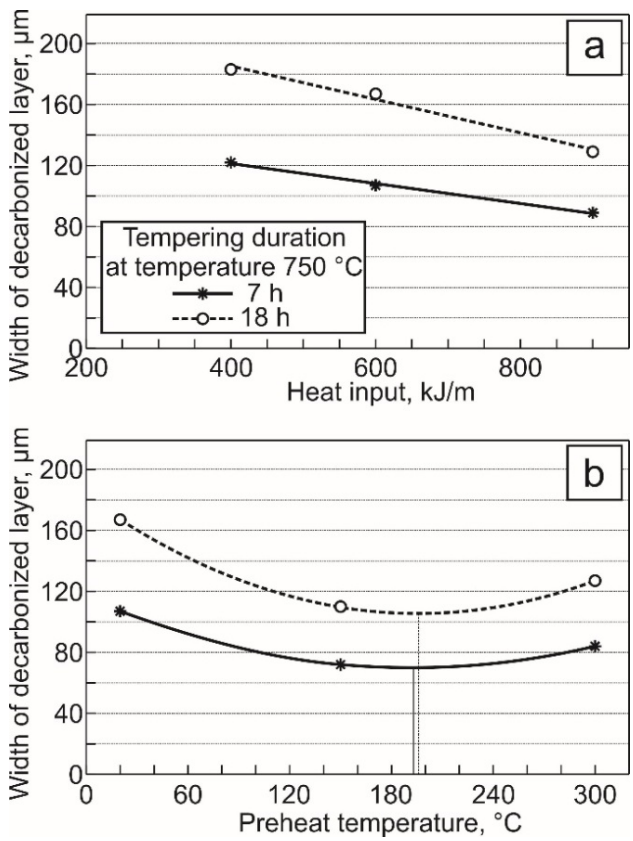

Fig. 5. Dependences of the average width of the decarburized layer on the welding parameters after tempering 750°C, 8 and 17 h

The theoretical basis of the obtained results is as follows: real steels contain a number of extended defects, including dislocations, grain boundaries, pores and surfaces. In general, the value of the diffusion coefficient D is scaled depending on the degree of freedom that the atom receives in the material. In most cases, the following ratio of diffusion coefficients is realized in the metal body [35, p. 135]:

$$D_{lattice} < D_{dislocation} < D_{grain\ boundary}$$

Lattice diffusion represents the most severe constraint to atomic migration, leading to the lowest diffusivities and the highest activation enthalpies in a given material. Due to their deformed structure, dislocations restrict atomic motion less than the lattice. High-angle grain boundaries with their less densely packed structure promote fast atomic diffusion [36, p. 549].

The activation energy for diffusion tends to decrease with decreasing constraint. Therefore, diffusion through defective regions becomes more important at lower temperatures. For example, grain boundary diffusion in polycrystalline materials plays a major role at temperatures below $0.6 \cdot T_{melting}$ [36, p. 548]. Examples of processes controlled mainly by grain boundary diffusion are diffusional creep, discontinuous precipitation, diffusion induced grain-boundary migration, recrystallization, and sintering.

While diffusion through defective areas may occur more rapidly than diffusion through defect-free material, the overall effect depends on the relative number (density) of extended defects in the solid. Reducing the diffusion rate can be achieved by increasing the grain size (diameter), which reduces the total area of the grain boundaries per unit volume. At relatively low temperatures, such as operating temperatures in thermal power plants, diffusion due to defects (grain boundaries, dislocations) is of paramount importance, so reducing the area of grain boundaries leads to a significant reduction in diffusion rate.

Bearing in mind the above theses, the obtained results can be explained as follows:

1) With the increased heat input or with preheating we obtain the more gentle sloping welding thermal cycle, which causes longer stay of metal of a weld-adjacent zone at temperatures of grain growth; the result is the formation of a large grains area in the weld-adjacent zone, which should more inhibit the carbon diffusion during PWHT and high-temperature operation.
2) It is known that in the presence of a temperature gradient during recrystallization, grain growth occurs in the direction of this gradient [37], which in the case of a welded joint can lead to the growth of grains in the direction perpendicular to the fusion surface. In the

presence of preheating, heat dissipation into the base metal is reduced, so in this case the grains in the weld-adjacent zone of the HAZ should be formed more equiaxed.

From geometric point of view, a carbon atom, which have to pass the same path along a boundary of elongated or equiaxed grains, has a greater displacement from fusion line at the end of elongated grain than at the end of equiaxed grain (Fig. 6). So approximately equal amount of carbon should migrate from the layer of width L1 in the weld-adjacent zone with elongated grains as from the layer of width L2 in the weld-adjacent zone with equiaxed grains, which led to larger decarburization in the former case at the same high temperature exposure time.

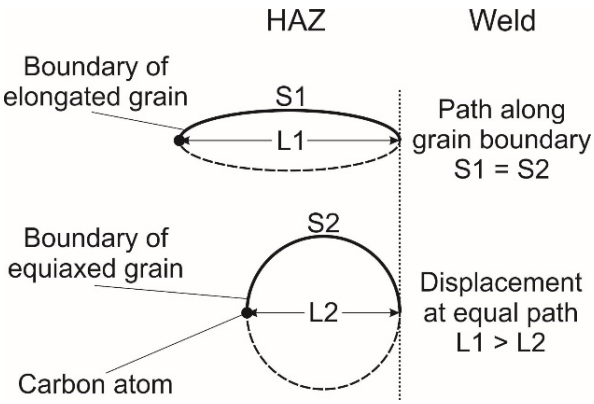

Fig. 6. Comparison of the distance of displacement of diffusing atoms depending on the geometry of the grains in the HAZ

The increase in the width of the decarburized layer at temperatures above 195°C can be explained by the overall intensification of the initial diffusion in HAZ in the state after welding with increasing preheat temperature (in this case the weldment has longer exposure time at high temperatures), when the gain in grain size and their equiaxity, obtained at moderate preheat temperatures, ceases to play a significant role.

The dependence of the width of the decarburized layer on the duration of exposure at a constant temperature has a parabolic form [38-40]: $P^2 = a \cdot t$, where P is the width of the layer (μm), t is the duration of exposure at a certain temperature (h); a – constant, which includes the diffusion coefficient. Having data on the width of the layer at 7 and 18 hours of exposure, a graph of inverse parabolic function

$$P = \sqrt{a} \cdot \sqrt{t} \quad (3)$$

obtained by approximation of the data with the nonlinear least squares method, was prepared (Fig. 7). The values of the determined parameters $\sqrt{a}$ ranged from 25.33 (for the conditions I_{weld} = 120 A, $T_{preheat}$ = 195°C) to 43.97 (for the conditions I_{weld} = 100 A, $T_{preheat}$ = 20°C).

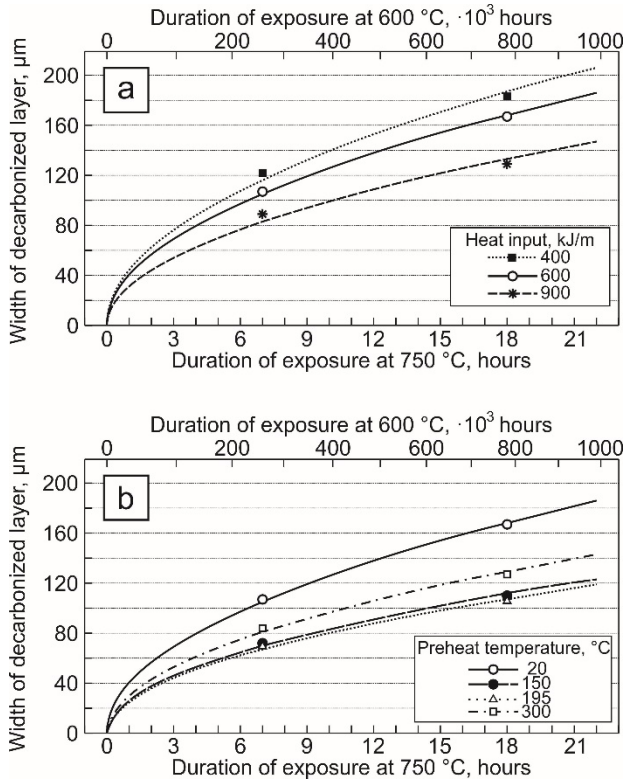

Fig. 7. Dependence of the width of decarbonized layers on duration of exposure time at temperatures 750°C and 600°C (approximating by Larson-Miller parameter) with variation of heat input (a) and preheat temperature (b)

For comparison, the graph above shows a logarithmic scale of exposure times at 600°C (normal operating temperature of P91 + austenitic steel joints in power plants), which correspond to exposures at 750°C, constructed using the Larson-Miller parameter [41]:

$$P = T \cdot (\log(t) + C)$$

where T is the absolute exposure temperature (K), t is the exposure time (h), C = 25.74 for steel 9Cr-1Mo-VNb type [41]. To calculate the duration of exposure at 600°C the equation was solved:

$$1023 \cdot (\log(t_{750°C}) + 25.74) = 873 \cdot (\log(t_{600°C}) + 25.74) \quad (4)$$

An approximate estimate of the obtained data indicates that in the welded joints of P91 + austenitic steel, first tempered at 750°C, 3 h, and then operated at 600°C,

100000 h, in HAZ of steel P91 will be observed a certain difference in the width of the decarbonized layer depending on welding conditions: a joint, welded on low current without preheating and with high heat dissipation, will have a layer approximately 1.75 times larger than a joint, welded on medium current with constant pre- and concurrent heating ~200°C; even a joint, welded with constant overheating to 300°C, will have a layer ~1.25 times larger than when preheated to ~200°C. With a longer duration of PWHT, the difference in the width of the layer, depending on welding conditions, will be even greater.

With an increase in heat input energy and use of optimized temperatures of pre- and concurrent heating, man can achieve a significant inhibition of the development of decarburization in the weld-adjacent area of HAZ in dissimilar welded joints. However, usually the use of steels with increased grain size is constrained by design conditions, as well as the use of welding conditions with high input energy and electrodes with suboptimal alloying. Therefore, the main factors may include the selection of the optimal heat input energy, which does not lead to decrease in ductility and formation of other defects, such as temper cracks, and optimization of the pre- and concurrent heating conditions.

3. Conclusions

1. It is determined that the width of the decarburized layer in P91 steel (welded with austenitic welding material), which develops during PWHT or high-temperature operations, can be varied by changing the values of heat input energy and pre-/concurrent heating of the welding conditions: the layer decreases with increase of heat input energy and decreases to ~195°C and then increases with increase of heating temperature (parabolic dependence).
2. The inverse parabolic curves of the layer width with increasing exposure time at the temperature of 750°C have been presented depending on the welding conditions.

References

[1] A. Di Gianfrancesco (ed.), Materials for Ultra-Supercritical and Advanced Ultra-Supercritical Power Plants, Woodhead Publishing, 2017.

[2] S. Huysmans, J. Vekeman, C. Hautfenne, Dissimilar metal welds between 9Cr creep strength enhanced ferritic steel and advanced stainless steels—creep rupture test results and microstructural investigations, Welding in the World 61 (2017) 341-350. DOI: https://doi.org/10.1007/s40194-016-0414-9

[3] R.J. Christoffel, R.M. Curran, Carbon migration in welded joints at elevated temperatures, Welding Journal 35/9 (1956) 457-468.

[4] K. Laha, K.S. Chandravathi, K. Bhanu Sankara Rao, S.L. Mannan, D.H. Sastry, An assessment of creep deformation and fracture behavior of 2.25Cr–1Mo similar and dissimilar weld joints, Metallurgical and Materials Transactions A 32 (2001) 115-124. DOI: https://doi.org/10.1007/s11661-001-0107-9

[5] C.D. Lundin, K.K. Khan, D. Yang, Effect of carbon migration in Cr-Mo weldments on metallurgical structure and mechanical properties, Welding Research Council Bulletin 407 (1995) 1-49.

[6] J. Dobrzański, A. Zieliński, H. Krztoń, Mechanical properties and structure of the Cr-Mo-V low-alloyed steel after long-term service in creep condition, Journal of Achievements in Materials and Manufacturing Engineering 23/1 (2007) 39-42.

[7] G.D. Pigrova, B.S. Kabanov, V.M. Sedov, The effect of long-term service on carbide transformations in Cr-Mo steels, Proceedings of the Proceedings of the 11th International Scientific Conference "Achievements in Mechanical and Materials Engineering", AMME'2002, Gliwice-Zakopane, 2002, 439-442.

[8] C. Sudha, A.L.E. Terrance, S.K. Albert, M. Vijayalakshmi, Systematic study of formation of soft and hard zones in the dissimilar weldments of Cr-Mo steels, Journal of Nuclear Materials 302/2-3 (2002) 193-205. DOI: https://doi.org/10.1016/S0022-3115(02)00777-8

[9] R. Anand, C. Sudha, T. Karthikeyan, A.L.E. Terrance, S. Saroja, M. Vijayalakshmi, Effectiveness of Ni-based diffusion barriers in preventing hard zone formation in ferritic steel joints, Journal of Materials Science 44 (2009) 257-265. DOI: https://doi.org/10.1007/s10853-008-3052-9

[10] H. Heuser, C. Jochum, W. Bendick, B. Hahn, Welding of dissimilar joints of new power plant steels, Proceedings of the IIW International Conference Safety and Reliability of Welded Components in Energy and Processing Industry, Graz, Austria, 2008, 217-223.

[11] T. Helander, C. Henrik, M. Andersson, M. Oskarsson, Structural changes in 12-2.25% Cr weldments - an experimental and theoretical approach, Materials at High Temperature 17/3 (2000) 389-396. DOI: https://doi.org/10.1179/mht.2000.17.3.003

[12] A. Varma, R.K. Yadavalli, Failure analysis of a reheater tube dissimilar metal weld failure in a 500 MW power plant, Engineering Failure Analysis 118 (2020) 104851. DOI: https://doi.org/10.1016/j.engfailanal.2020.104851
[13] S.J. Brett, Type IIIa cracking in 1/2CrMoV steam pipework systems, Science and Technology of Welding and Joining 9/1 (2004) 41-45. DOI: https://doi.org/10.1179/136217104225017134
[14] D. Gandy, K. Coleman, Performance Review of T/P91 Steels, EPRI, Palo Alto, CA, 2002, 1004516.
[15] J. Frei, B.T. Alexandrov, M. Rethmeier, Low heat input gas metal arc welding for dissimilar metal weld overlays part III: hydrogen-assisted cracking susceptibility, Welding in the World 63 (2019) 591-598. DOI: https://doi.org/10.1007/s40194-018-0674-7
[16] D. Bourgeois, Hydrogen assisted crack in dissimilar metal welds for subsea service under cathodic protection, PhD Thesis, The Ohio State University, 2015.
[17] J.A. Fenske, I.M. Robertson, R. Ayer, M. Hukle, D. Lillig, B. Newbury, Microstructure and hydrogen-induced failure mechanisms in Fe and Ni alloy weldments, Metallurgical and Materials Transactions A 43 (2012) 3011-3022. DOI: https://doi.org/10.1007/s11661-012-1129-1
[18] Y.Y. You, R.K. Shiue, R.H. Shiue, C. Chen, The study of carbon migration in dissimilar welding of the modified 9Cr-1 Mo steel, Journal of Materials Science Letters 20 (2001) 1429-1432. DOI: https://doi.org/10.1023/A:1011616232396
[19] R. Anand, C. Sudha, V.T. Paul, S. Saroja, Microstructural changes in Grade 22 ferritic steel clad successively with Ni-based and 9Cr filler metals, Welding Journal 89 (2010) 65s-74s.
[20] M. Sireesha, S.K. Albert, S. Sundaresan, Thermal cycling of transition joints between modified 9Cr-1Mo steel and Alloy 800 for steam generator application, International Journal of Pressure Vessels and Piping 79/12 (2002) 819-827. DOI: https://doi.org/10.1016/S0308-0161(02)00104-7
[21] K. Karthick, S. Malarvizhi, V. Balasubramanian, A. Gourav Rao, Tensile properties variation across the dissimilar metal weld joint between modified 9Cr-1Mo ferritic steel and 316LN stainless steel at RT and 550°C, Metallography, Microstructure and Analysis 7 (2018) 209-221. DOI: https://doi.org/10.1007/s13632-018-0430-9
[22] M. Urzynicok, R. Jachym, K. Kwiecinski, P. Mariani, Y. Minami, Application of EPRI87 in dissimilar welding austenitic-martensitic welded joints of TEMPALOY AA-1 and T92 steel grades, Proceedings of the 7th International Conference Advances in Materials Technology for Fossil Fuel Power Plants, Waikoloa, Hawaii, USA, 2013, 992-1005.
[23] K. Coleman, D. Gandy, Alternative filler materials for DMWs involving P91 materials, Proceedings of the 5th International Conference Advances in Materials Technology for Fossil Fuel Power Plants, Marco Island, Florida, USA, 2007, 940-967.
[24] S. Mahajan, R. Chhibber, Investigations on dissimilar welding of P91/SS304L using Nickel-based electrodes, Materials and Manufacturing Processes 35/9 (2020) 1010-1023. DOI: https://doi.org/10.1080/10426914.2020.1755041
[25] C. Pandey, J.G. Thakare, P.K. Taraphdar, P. Kumar, A. Gupta, S. Sirohi, Characterization of the soft zone in dissimilar welds joint of 2.25Cr-1Mo and lean duplex LDX2101 steel, Fusion Engineering and Design 163 (2021) 112147. DOI: https://doi.org/10.1016/j.fusengdes.2020.112147
[26] S. Kumar, S. Sirohi, R.S. Vidyarthy, A. Gupta, C. Pandey, Role of the Ni-based filler composition on micro-structure and mechanical behavior of the dissimilar welded joint of P22 and P91 steel, International Journal of Pressure Vessels and Piping 193 (2021) 104473. DOI: https://doi.org/10.1016/j.ijpvp.2021.104473
[27] G. Dak, C. Pandey, A critical review on dissimilar welds joint between martensitic and austenitic steel for power plant application, Journal of Manufacturing Processes 58 (2020) 377-406. DOI: https://doi.org/10.1016/j.jmapro.2020.08.019
[28] S. Singh, A.B. Singh, M. Kumar, M.L. Meena, G.S. Dangayach, Dissimilar Metal Welds used in AUSC Power Plant: Fabrication and Structural Integrity Issues, IOP Conference Series: Materials Science and Engineering 1017 (2021) 012022. DOI: https://doi.org/10.1088/1757-899X/1017/1/012022
[29] D.D. Awale, A.R. Ballal, M.M. Thawre, Dissimilar weld joints of P91 and 316LN for power plants Applications-A review, Materials Today: Proceedings 28/4 (2020) 2505-2510. DOI: https://doi.org/10.1016/j.matpr.2020.05.003
[30] A.K. Maurya, C. Pandey, R. Chhibber, Dissimilar welding of duplex stainless steel with Ni alloys: A review, International Journal of Pressure Vessels and Piping 192 (2021) 104439. DOI: https://doi.org/10.1016/j.ijpvp.2021.104439
[31] S. Sirohi, C. Pandey, A. Goyal, Role of the Ni-based filler (IN625) and heat-treatment on the mechanical performance of the GTA welded dissimilar joint of P91 and SS304H steel, Journal of Manufacturing Processes 65 (2021) 174-189. DOI: https://doi.org/10.1016/j.jmapro.2021.03.029

[32] S. Sirohi, C. Pandey, A. Goyal, Characterization of structure-property relationship of martensitic P91 and high alloy ferritic austenitic F69 steel, International Journal of Pressure Vessels and Piping 188 (2020) 104179.
DOI: https://doi.org/10.1016/j.ijpvp.2020.104179
[33] Y.M. Lakhtin, Physical metallurgy and heat treatment, Third Edition, Metallurgy, Moscow, 1984 (in Russian).
[34] ImageJ. Image Processing and Analysis in Java. Available from: https://imagej.nih.gov/ij/
[35] R. O'Hayre, Materials kinetics fundamentals: principles, processes, and applications, Wiley, 2015.
[36] H. Mehrer, Diffusion in Solids: Fundamentals, Methods, Materials, Diffusion-Controlled Processes, Springer-Verlag, Berlin-Heidelberg, 2007. DOI: https://doi.org/10.1007/978-3-540-71488-0
[37] Y. Ushigami, T. Kumano, T. Haratani, S. Nakamura, S. Takebayashi, T. Kubota, Secondary Recrystallization in Grain-Oriented Silicon Steel, Materials Science Forum 467-470 (2004) 853-862. DOI: https://doi.org/10.4028/www.scientific.net/MSF.467-470.853
[38] M. Zorc, A. Nagode, J. Burja, B. Kosec, B. Zorc, Surface Decarburization of the Hypo-Eutectoid Carbon Steel C45 during Annealing in Steady Air at Temperatures T > A_{C1}, Metals 8/6 (2018) 425. DOI: https://doi.org/10.3390/met8060425
[39] D. Li, D. Anghelina, D. Burzic, W. Krieger, E. Kozeschnik, Investigation of Decarburization in Spring Steel Production Process – Part II: Simulation, Steel Research International 80/4 (2009) 304-310. DOI: https://doi.org/10.2374/SRI08SP070
[40] J. Konieczny, Z. Rdzawski, P. Bańbura, B. Preficz, Influence of aging time and temperature on diffusion of alloyed copper, Journal of Achievements in Materials and Manufacturing Engineering 73/1 (2015) 27-35.
[41] M. Tamura, F. Abe, K. Shiba, H. Sakasegawa, H. Tanigawa, Larson–Miller Constant of Heat-Resistant Steel, Metallurgical and Materials Transactions A 44/6 (2013) 2645-2661.
DOI: https://doi.org/10.1007/s11661-013-1631-0

© 2021 by the authors. Licensee International OCSCO World Press, Gliwice, Poland. This paper is an open access paper distributed under the terms and conditions of the Creative Commons Attribution-NonCommercial-NoDerivatives 4.0 International (CC BY-NC-ND 4.0) license (https://creativecommons.org/licenses/by-nc-nd/4.0/deed.en).